I–V Data Operated High-Quality Photovoltaic Solution Through Per-Unit Single-Diode Model

Ashish K. Panchal, *Member, IEEE*

***Abstract*—The work presented here uses a novel photovoltaic (PV) parameter extraction method that uses the generalized per-unit single-diode model (PUSDM) of a PV module. In the first extraction stage, the PUSDM is approximated as an explicit nonlinear model (EXNLM). The EXNLM utilizes the experimental current–voltage (*I–V*) data of a PV module to estimate initial guesses. The second stage exploits the PUSDM with reduced parameters and extracts the three parameters using the nonlinear least-square-fit (NLLSF) technique. The third stage refines the five parameters using the original PUSDM. Here, again the NLLSF is employed using the solution obtained in the second stage as the initial guesses. The proposed method is tested on the experimental and synthetic *I–V* curves of several silicon PV cells and modules commonly available in the PV literature using MATLAB programming platform. The high-quality PV solution is obtained with the least computational cost ever published in the PV literature. The other salient features of the work are: 1) an ability to work without the PV module key operating points, 2) a self-computation of the initial guesses, and 3) an ability to work with the partial *I–V* data points. Most importantly, the MATLAB-script of the proposed method is made available for ready-use through e-mail.**

***Index Terms*—Current–voltage (*I–V*) curve, Lambert W function, parameter extraction, per-unit (p.u.) computation, single-diode model (SDM), silicon photovoltaic (PV) module.**

I. Introduction

ENORMOUS development in the photovoltaic (PV) power technologies frequently demands the PV modeling tools for online maximum power point (MPP) monitoring, PV system designs, PV module degradation, and failure studies [1]. A single-diode model (SDM) also referred as a five parameter model is commonly used in the PV modeling [2]. The SDM is widely adopted in the PV studies because of its scalability to represent a small PV cell to a wide area PV array with simplicity and its capability to demonstrate the performance of a PV module in different atmospheric conditions (varying solar irradiance, temperature, and partial shading) [3].

The SDM features the PV module output characteristic in terms of the current–voltage (*I–V*) and the five circuit parameters. In the aforementioned PV studies, many times the inverse PV modeling is essential in which the five parameters are extracted. A common approach for the parameter extraction is that it make use of the manufacturer datasheet information such as the short-circuit current ($I_{\rm SC}$), the open-circuit voltage ($V_{\rm OC}$), and the MPP [4]. With the help of the reference parameters obtained by this approach, one can predict the PV performance in different atmospheric conditions. Some works of literature cite a different approach that uses experimental *I–V* curve of a module [5], [6]. The parameter extraction is performed using the least-square-fit (LSF) technique that minimizes the squared error between the estimated current and the measured current [7]. This has two-fold benefits: 1) it provides a high-quality solution and 2) it makes the study of PV parameter dependency on the different environmental conditions possible.

The experimental *I–V* curve-driven PV solution of the SDM is a nonconvex optimization problem [8]. This problem is hard to such an extent that the deterministic algorithms (such as trust-region and Levenberg–Marquardt) used for the solution are trapped in a local minimum. In fact, changing the initial guesses for the solution returns a different local minimum. Thus, the existence of a number of local minima does not allow the direct use of the deterministic algorithms and the solution to the global optimum is not possible. However, in order to obtain the global optimum solution, several stochastic algorithms inspired by the artificial intelligence are recently adopted such as the teaching-learning-based optimization [9], adaptive wind-driven optimization [10], improved brainstorming optimization [11], hybrid form of analytical and simulated annealing optimization [12], onlooker-ranking-based adaptive differential optimization [13], improved moth-flame-optimization [14], genetic algorithm [15], etc. Although these algorithms reach to the global optimum solution, the convergence time and computation costs (CC) are very high and result in slightly inferior quality solutions than the deterministic algorithms. Indeed, the aforementioned difficulty is overcome by transforming the five (parameters) dimensions (5-D) search problem to the reduced dimensions (2-D/3-D) search [16]. The reduced dimensions search problem converts the original nonconvex problem into the convex one, and allow the use of the deterministic algorithms. In addition, the high-quality PV solution is achieved with a great reduction in computational time and costs.

Recently, a few works of literature [17]–[21] have attempted the PV solution based on the reduced dimensions search and the LSF technique. In [17], for various PV technologies, the problem is reduced from 5-D to 3-D with the help of the additional data points ($I_{\rm SC}$, $V_{\rm OC}$, and the MPP). However, the accuracy

Manuscript received March 26, 2020; revised May 11, 2020; accepted May 18, 2020. Date of current version June 19, 2020.

The author is with the Department of Electrical Engineering, S V National Institute of Technology, Surat 395007, India (e-mail: akp@eed.svnit.ac.in).

This paper has supplementary downloadable material available at https://ieeexplore.ieee.org provided by the author.

Color versions of one or more of the figures in this article are available online at https://ieeexplore.ieee.org.

Digital Object Identifier 10.1109/JPHOTOV.2020.2996711

is not satisfactory because of several assumptions made in the method. In [18], the problem is reduced to the 2-D search wherein two different reduced forms are proposed using the additional module operating data points. However, the solution obtained by both forms is not unique and sensitive to the initial guesses. The methods, which need additional operating data points, influence the quality of the solution as the additional data are roughly estimated in many cases. In another literature [19] with a similar 2-D search problem, the reduced form is obtained by an educated approximation and employing the generalized Bender-like decomposition. The method works fully automated without the additional operating data points and with the same accuracy and less CC than in [18]. It is to note that all three methods use the nonlinear LSF (NLLSF) technique. Other two methods [20], [21] have come up with the linear-LSF (LLSF) technique to solve the nonlinear PV optimization problem. In [20], the PV optimization problem is seen as a linear system whose parameters are linked with a set of linear differential equations that can be easily solved by the LLSF technique. Though the problem dimension is reduced from 5-D to 1-D, the accuracy is not the same as the best documented in [18] and [19]. In [21], the *I–V* curve is divided into two parts: the linear and the exponential. Both the parts are converted into the sets of linear equations and subsequently are solved using the LLSF technique. Since the LLSF technique does not need initial guesses, the methods work completely blindly without additional module operating data points.

The present work highlights a specific point used by all the methods discussed previously. All of them use the electrical quantities in the SDM with their real units, e.g., I is expressed in Amperes (A), V is in Volts (V), and $R_s/R_{\rm sh}$ are in Ohms (Ω). This article first time introduces a per-unit SDM (PUSDM) in which all the quantities are expressed with respect to their base values. The per-unit computation concept is adopted from the electrical power system analysis [22]. The PUSDM helps in reducing the CC as discussed later.

Here, the 5-D search problem is reduced to 3-D, as demonstrated in [17] using the PUSDM without any approximations. The PV solution procedure is divided into three stages: 1) the computation of the initial guesses, 2) the PV parameter estimation using the 3-D PUSDM, and 3) the PV parameter refinement using the 5-D PUSDM. In the stage-I, the PUSDM is converted into an explicit nonlinear model (EXNLM). The EXNLM estimates the initial guesses. The PUSDM with the 3-D search form is exploited to solve the problem using NLLSF technique in the stage-II. Finally, the PV solution is refined with the help of the PUSDM in the 5-D search form using the NLLSF technique and the solution obtained in the stage-II as the initial guesses. The proposed method is tested on commonly used case studies with the full *I–V* curves. The high-quality solution is found with the least CC ever published in the literature until now.

During the online MPP tracking, the power converters connected to the PV module do not allow to measure $I_{\rm SC}$ and $V_{\rm OC}$ in order to reduce the power losses and to avoid the interruption in the PV operation. On the other hand, the SDM parameters are required to estimate the MPP. The converter allows to measure limited *I–V* data points near to the MPP. In such a situation, the methods [17] and [18], which need the specific operating points along with the *I–V* curve, fail to provide the solution. While the other methods [19]–[21], which blindly work with only the *I–V* curve provide the PV solution with significant CC. The present method also addresses this situation considering the partial *I–V* curves of the same four case studies. The best PV solution is obtained with a significant reduction in CC.

Additionally, the performance of the present method is analyzed on the synthetic *I–V* curves of four PV modules generated by known five parameters. The PV solutions for these curves are highly accurate and obtained with the least computational costs. The present method needs an operating temperature together with an input *I–V* curve. However, Lappalainen *et al.* [23] and Giovanni *et al.* [24] have very recently published methods that extract the five parameters along with the irradiance and temperature conditions.

The rest of this article is organized as follows: Section II includes the derivation of the PUSDM from the SDM. Section III explains the complete PV solution procedure in the form of the stage-I, -II, and -III using the PUSDM. Section IV includes the results of the case studies obtained by the present method and its comparison with the previously published results. In this section, the case studies are analyzed with the full and partial *I–V* curves. Section V illustrates the parameter extraction for the synthetic curves under STC and non-STC conditions. Finally, Section VI lists the key features of the present method.

II. Per-Unit Single-Diode Model

The well-known SDM representation of a PV module for a given solar irradiance and temperature is written as [2]

$$I = I_{ph} - I_0 \left\{ \exp\left(\frac{V + IR_s}{V_t} \right) - 1 \right\} - \frac{(V + IR_s)}{R_{\rm sh}} \quad (1)$$

where I_{ph} = the light current, I_0 = the reverse saturation current, R_s = the series resistance, $R_{\rm sh}$ = the shunt resistance, V_t = the thermal voltage $= N_s nkT/q$ with N_s = the number of cells connected in series in a module, n = the diode ideality factor, k = the Boltzmann constant $= 1.3806503 \times 10^{-23}$ J/K, T = the cell temperature in °C ($= 273.15 + T$ in K), and q = the electron charge $= 1.602 \times 10^{-19}$ C. Here, the problem in hand is to obtain the PV solution, i.e., the extraction of the five parameters (I_{ph}, I_0, n, R_s, and $R_{\rm sh}$) that best fits the given *I–V* curve with the SDM.

In the proposed method, the parameter extraction procedure begins with only one input data, i.e., an experimentally measured *I–V* curve of a PV module, without additional information such as $I_{\rm SC}$, $V_{\rm OC}$, and the MPP. In general, the experimental measurements provide a full *I–V* curve (in some cases extended beyond the positive *I–V* plane as illustrated by the case studies later) or a partial one (the curve measured near the MPP). These measurements never provide previously mentioned additional information. Therefore, the PUSDM is developed in such a way that it can deal with any kind of *I–V* curve. The *I–V* curve is a set of N data points, (V_1, I_1), $(V_2, I_2), \ldots\ldots, (V_N, I_N)$. In order to obtain the PV solution in the per-unit (p.u.), the input data has to be converted into p.u. The p.u. computation starts with a selection of base quantities. From the data set,

the highest voltage ($V_N = V_H$) and the highest current ($I_1 = I_{\rm H}$) are selected as a base. Dividing the input data with their corresponding base values, the p.u. input data take the form, (v_1, 1), (v_2, i_2), …… ….., (1, i_N). It is made clear that two extreme points (v_1, 1) and (1, i_N) are redenoted as (v_{IH}, 1) and (1, i_{VH}), respectively, for understanding purpose, where v_{IH} is the p.u. voltage for the highest current and i_{VH} is the p.u. current for the highest voltage. In addition, a base value to represent the resistances in the SDM is chosen as $R = V_H/I_H$. The SDM conversion to the PUSDM is obtained by dividing the base values in (1) as

$$\frac{I}{I_H} = \frac{I_{ph}}{I_H} - \frac{I_0}{I_H}\left\{\exp\left(\frac{\frac{V}{V_H} + \frac{I}{I_H}R_s\frac{I_H}{V_H}}{\frac{V_t}{V_H}}\right) - 1\right\} - \frac{\left(\frac{V}{V_H} + \frac{I}{I_H}R_s\frac{I_H}{V_H}\right)}{R_{\rm sh}\frac{I_H}{V_H}}. \tag{2a}$$

With the p.u. quantities, $V/V_H = v =$ the p.u. voltage, $I/I_H = i =$ the p.u. current, $I_{ph}/I_H = i_{ph} =$ the p.u. light current, $I_0/I_H = i_0 =$ the p.u. reverse saturation current, $R_s/R = r_s =$ the p.u. series resistance, and $R_{\rm sh}/R = r_{\rm sh} =$ the p.u. shunt resistance, (2a) is rearranged to give the following general form of the PUSDM:

$$i = \frac{i_{ph}}{r} - \frac{i_0}{r}\left\{\exp\left(b\left(v + ir_s\right)\right) - 1\right\} - \frac{v}{rr_{\rm sh}} \tag{2b}$$

where $b = V_H/V_t$ and $r = 1 + (r_s/r_{\rm sh})$. The PV solution to obtain the five parameters using (2) is referred as the 5-D PUSDM. At this step, it is worth noticing that the solution of the PUSDM returns the five parameters in p.u., and they have to be multiplied by their respective base values to obtain the parameters in their actual units.

With an aim to perform the parameter extraction with the 3-D search as in [17], the 5-D PUSDM in (2b) is reduced to the 3-D PUSDM. In order to do so, the two parameters (i_{ph} and i_0) are eliminated from (2b) with the help of two extreme data points, (v_{IH}, 1) and (1, i_{VH}), of the *I–V* curve. As a consequence, the substitution of both points in (2b) generates the following expressions for i_0 and i_{ph}:

$$\frac{i_0}{r} = \frac{(i_{VH} - 1) - \frac{(v_{IH}-1)}{rr_{\rm sh}}}{\exp\left(b\left(v_{IH} + r_s\right)\right) - \exp\left(b\left(1 + i_{VH}r_s\right)\right)} \text{ and} \tag{3}$$

$$\frac{i_{ph}}{r} = 1 + \frac{v_{IH}}{rr_{\rm sh}} + \frac{(i_{VH} - 1) - \frac{(v_{IH}-1)}{rr_{\rm sh}}}{\exp\left(b\left(v_{IH} + r_s\right)\right) - \exp\left(b\left(1 + i_{VH}r_s\right)\right)} \times \left(\exp\left(b\left(v_{IH} + r_s\right)\right) - 1\right). \tag{4}$$

The substitution of (3) and (4) into (2) yields the 3-D PUSDM for *i*, which is the function of the other three parameters (*n*, r_s, and r_{sh}). As a result, the 3-D PUSDM of (2b) becomes

$$i = 1 + \frac{(v_{IH} - v)}{rr_{\rm sh}} + \left((i_{VH} - 1) - \frac{(v_{IH} - 1)}{rr_{\rm sh}}\right) \times \frac{\left(\exp\left(b\left(v_{IH} + r_s\right)\right) - \exp\left(b\left(v + ir_s\right)\right)\right)}{\left(\exp\left(b\left(v_{IH} + r_s\right)\right) - \exp\left(b\left(1 + i_{VH}r_s\right)\right)\right)}. \tag{5}$$

The next step is the parameter extraction by fitting the *I–V* curve with the 3-D PUSDM using the NLLSF technique and associated three initial guesses.

III. PV Parameter Estimation With the PUSDM

A. Computation of the Initial Guesses: Stage-I

The first initial guess for *n* is estimated by generating an approximate EXNLM of the 3-D PUSDM of (5). The common assumptions of the terms $\exp(b(v_{IH} + r_s)) \gg \exp(b(v + ir_s))$ and $\exp(b(v_{IH} + r_s)) \gg \exp(b(1 + i_{VH}r_s))$ in (5) are valid for a silicon cell/module [25] and, thus, (5) is reformulated as

$$i = 1 + \frac{(v_{IH} - v)}{rr_{sh}} + \left((i_{VH} - 1) - \frac{(v_{IH} - 1)}{rr_{\rm sh}}\right) \times \exp\left(b\left(v - 1 + (i - i_{VH})\, r_s\right)\right). \tag{6}$$

Furthermore, the term $(i - i_{VH})r_s$ in (6) is neglected and (6) is transformed into

$$i = 1 + \frac{(v_{IH} - v)}{rr_{\rm sh}} + \left((i_{VH} - 1) - \frac{(v_{IH} - 1)}{rr_{\rm sh}}\right) \times \exp\left(b\left(v - 1\right)\right). \tag{7}$$

Understanding simple mathematics for the cells and modules, i.e., $v < 1$ (the p.u. value) and hence $-1 < (v - 1) < 0$, and hence, the last term in (7) can be written as, $\exp((v-1)b) \approx (1 + v - 1)^b = v^b$, (due to the fact that $\exp(x) \approx (1 + x)$ for $-1 < x < 0$) [26]. Therefore, (7) is translated into the following EXNLM:

$$i = d + cv + av^b. \tag{8}$$

In order to find n_0, the EXLNM of (8) is solved for *b* using two extreme data points (v_{IH}, 1), (1, i_{VH}), the MPP (v_m, i_m), and its slope. These four boundary conditions satisfy (8) and result in the following set of equations:

$$i_{VH} = a + c + d \tag{9a}$$

$$1 = av_{IH}^b + cv_{IH} + d \tag{9b}$$

$$i_m = av_m^b + cv_m + d \tag{9c}$$

$$0 = a\left(b + 1\right)v_m^b + cv_m + d. \tag{9d}$$

Equation (9) is solved using *fsolve* command in MATLAB with help of the following initial guesses to be assumed for *a*, *b*, *c*, and *d*

$$b_0 = \frac{V_H}{V_t} \tag{10a}$$

$$d_0 = 1 \tag{10b}$$

$$a_0 = \frac{d_0 - 2i_m}{\left(b_0 - 1\right)v_m^{b_0}} \tag{10c}$$

$$c_0 = \frac{i_m - d_0 - av_m^b}{v_m}. \tag{10d}$$

The *b* value evaluated in (9) gives the initial values of n_0 as

$$n_0 = \frac{V_H q}{bN_s kT}. \tag{11a}$$

For the other two initial guesses r_s and $r_{\rm sh}$, a common way is to assign the slopes *dv*/*di* of the *I–V* curve at the OC and the SC points, respectively [27]. Since the proposed method works without $V_{\rm OC}$ and $I_{\rm SC}$, it is not possible to assign the slopes for the initial guesses. Therefore, the proposed method adopts a different way to assign the initial guesses for these two parameters. For example, r_{s0} is set to the slope of the last two points of the *I–V* curve, (v_{N-1}, i_{N-1}) and $(v_N, i_N) = (1, i_{VH})$. The expression for r_{s0} is given by

$$r_{s0} = -\left(\frac{v_{N-1}-1}{i_{N-1}-i_{VH}}\right) \text{ and} \tag{11b}$$

$r_{\rm sh0}$ is set to the slope of the first two points of the *I–V* data, $(v_1, i_1) = (v_{IH}, 1)$ and (v_2, i_2). The expression for $r_{\rm sh0}$ is given as

$$r_{\rm sh0} = -\left(\frac{v_2 - v_{IH}}{i_2 - 1}\right). \tag{11c}$$

With the initial values of three parameters obtained using (11), the stage-I completes. Here, the initial guesses are self-computed using the *I–V* curve without additional information about $V_{\rm OC}$ and $I_{\rm SC}$.

B. PV Parameter Estimation With 3-D PUSDM: Stage-II

The transcendental nature of (5) ($i = f(v, i)$) makes the 3-D PUSDM solution infeasible in an explicit way. The suitable way to overcome this difficulty is to use the Lambert W function, which projects *i* as a function of *v* ($i = f(v)$), also adopted in the recent literature [28]. Therefore, the 3-D PUSDM shown in (5) is converted into an explicit form using the Lambert W function. In general, the following form of equation is required to apply the Lambert W function [29]:

$$A\exp(X) + B(X) + C = 0. \tag{12a}$$

The solution of (12a) using the Lambert W function is given as follows:

$$X = -\text{LambertW}\left\{\frac{A}{B}\exp\left(-\frac{C}{B}\right)\right\} - \frac{C}{B}. \tag{12b}$$

Equation (12) helps in the 3-D PUSDM conversion of (5) into the explicit form. When (5) is rearranged in form of (12a), the following expression comparison is yielded:

$$X = b(v + ir_s) \tag{13a}$$

$$A = -br_s\left\{\frac{i_{VH} - 1 + \left(\frac{1-v_{IH}}{rr_{\rm sh}}\right)}{\exp(b(v_{IH}+r_s)) - \exp(b(1+i_{VH}r_s))}\right\} \tag{13b}$$

$$B = -1 \tag{13c}$$

$$C = bv + br_s\left\{1 + \frac{(v_{IH}-v)}{rr_{\rm sh}}\right\} + br_s\left\{i_{VH} - 1 + \left(\frac{1-v_{IH}}{rr_{\rm sh}}\right)\right\} \times\left\{\frac{\exp(b(v_{IH}+r_s))}{\exp(b(v_{IH}+r_s)) - \exp(b(1+i_{VH}r_s))}\right\}. \tag{13d}$$

With help of (13) and (12b), *i* is expressed in the explicit form as follows:

$$i = -\frac{v}{r_s} - \frac{1}{br_s}\text{LambertW}\left\{\frac{A}{B}\exp\left(-\frac{C}{B}\right)\right\} - \frac{1}{br_s}\left(\frac{C}{B}\right). \tag{14}$$

The intermediate PV solution (n, r_s, and r_{sh}) is obtained using the NLLSF technique. In the NLLSF, (14) is employed using *lsqnonlin* function and the initial guesses derived in the stage-I. Consequently, i_0 and i_{ph} are also computed using (3) and (4). As a result, a set of five parameters is available at the end of the stage-II.

C. PV Parameter Refinement With 5-D PUSDM: Stage-III

Considering the solution obtained in the stage-II as initial guesses, further refinement in the five parameters is possible by using the 5-D PUSDM of (2). Once again, the Lambert W function is adopted to transform (2) into the explicit form [29]. Equation (2) is rearranged in form of (12a) and the comparison yields the following variables:

$$X = b(v + ir_s) \tag{15a}$$

$$A = -br_s\frac{i_0}{r} \tag{15b}$$

$$B = -1 \tag{15c}$$

$$C = bv + \frac{br_s}{r}\left(i_{ph} + i_0 - \frac{v}{r_{\rm sh}}\right). \tag{15d}$$

With a new set of variables in (15), the expression for *i* is the same as (14). The refined PV solution is obtained using the NLLSF technique. Equation (14) is re-employed using *lsqnonlin* function and the initial guesses obtained in the stage-II. Since the order of the five parameters is different, the *lsqnonlin* requires larger iteration steps for the convergence. Instead in the present work, the logarithmic values of the initial guesses are supplied to the function. Hence, there is significant reduction in the computational cost. Just after the convergence, the actual parameters are obtained by transforming the converged value using exponential. Notice that the NLLSF provides the three parameters in the stage-II and the five parameters in the stage-III. The flowchart of the parameter extraction method based on the PUSDM is shown in Fig. 1, which gives the stage-III as an option.

IV. PV Solution With Experimental *I–V* Curves

Here, four case studies, commonly used in the PV literature, are examined by the proposed method: 1) Case study #1: the *I–V* curve of a 57-mm diameter RTC France silicon solar cell measured with 1000 W/m^2 and 33 °C [30], 2) Case study #2: the *I–V* curve of a polycrystalline silicon module Photowatt-PWP 201 (36 cells in series) measured with 1000 W/m^2 and 45 °C [30], 3) Case study #3: the *I–V* curve of a monocrystalline silicon module STM6-40 (36 cells in series) measured with 51 °C [31], and 4) Case study #4: the *I–V* curve of a polycrystalline silicon module STM6-120 (36 cells in series) measured with 55 °C [31]. Two sets of experimental *I–V* curves are used. In the first, the

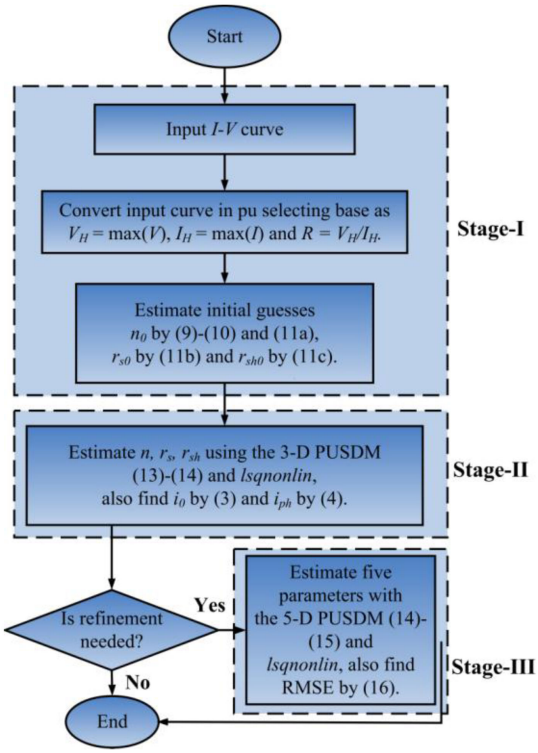

Fig. 1. Flowchart of the proposed method.

full *I–V* curves (denoted as *F* with the case studies number) of four case studies are used. In the second, the partial *I–V* curves (denoted as *P* with the case studies number) of the same four case studies are employed.

The method was performed on MATLAB R2014b using the in-built functions *fsolve* and *lsqnonlin*. The numerical computations were conducted on a Windows 7 Professional system (64-bits operating system) with an Intel (R) Core (TM) i7-3770 processor 3.40 GHz CPU and with 4 GB memory. Here, the accuracy of the methods is compared in terms of the root-mean-squared-error (RMSE) in the estimated current (I_{Ei}) and measured current (I_{Mi}). The RMSE is defined as follows:

$$\mathrm{RMSE} = \sqrt{\frac{1}{N}\sum_{i=1}^{N}(I_{Ei} - I_{Mi})^2}. \tag{16}$$

Since the PV solution method uses the NLLSF technique (use of *lsqnonlin* function in MATLAB), the method is compared in terms of CC such as the number of iteration steps and the function evaluations (FEs). In the present section, the style for presenting the CC is adopted as a number of the steps/number of FEs everywhere. For the comparison purpose, the numerical values of five parameters, RMSE, CC are used as they appear in the literature. The results for the present method are truncated to the same number of digits as presented in [21].

The present method is compared with the methods in Laudani *et al.* [18], Cárdenas *et al.* [19], and Toledo *et al.* [21]. In all, the PV solution is obtained in two stages, without and with refinement. In the first, the Laudani and Cárdenas methods use the 2-D SDM, whereas the present one uses the 3-D PUSDM. These three employ the NLLSF technique, hence require initial guesses and perform the computation in steps with FEs. On the other hand, the Toledo method needs the LLSF technique that provides a direct PV solution. In the second, all methods refine the PV solution using the 5-D SDM/PUSDM with the previous solution as initial guesses. Once again, the NLLSF technique requires initial guesses and performs the computation in steps with FEs. At this point, it is worth to note that the previous three methods have twice CC, whereas the Toledo method has only once.

A. PV Solution With Full I–V Curves

The discussion starts with the selection of the initial guesses. In [18], the n_0 value is selected in the range [0.5, 2.5] and subsequently the feasible R_s value is found using the MPP and the Lambert W function. In [19], the n_0 value is set to 5.0 and R_{s0} is set to $0.05 \times \{\max(V_k)/\max(I_k)\}$. Laudani *et al.* [16] use the 3-D SDM (with n, R_s, and R_{sh}) in which n_0 and R_{s0} are derived from the plot dV/dI verses $(I_{SC} - I - V/R_{\mathrm{sh}})^{-1}kT/q$, whereas R_{sh0} is defined by the slope dV/dI at I_{SC}. The present method uses a different way to find the initial guesses as follows. First $n = 1$ is selected and the EXNLM (9) and (10) computes the initial n_0 using (11a). The r_{sh0} and r_{s0} values are defined in (11a) and (11b), respectively, (noting that if any of the slopes is undefined then the immediate next slope is selected as in the case study #3F). Thus, three initial guesses are independently selected unlike [18]. Table I shows the base values for p.u. computation, the parameters obtained in the stage-I for all case studies. The d value near to 1 indicates I_{SC} of the PV devices, whereas $d = 1.00$ indicates the *I–V* curve starts with I_{SC} otherwise the curve is extended in the negative *V*-axis or the partial curve. It is worth to note that the variation in b in the range 7–12 results in n to vary within 1–2.5.

Table II lists the PV solution without refinement, i.e., the five parameters (in p.u. and actual unit), the RMSE, the CC, obtained using the 3-D PUSDM for the case studies #1F and #2F, and compares with those obtained by the 2-D SDM shown in [18] and [19]. It is observed that the RMSE by the present method is of a similar order. For both the case studies, a small deviation is observed in the five parameters obtained by the present method and hence the RMSE differs with respect to the values of other methods. Also, a small difference exists in the CC. These differences are obvious because the present method is based on the 3-D PUSDM, whereas the other two are based on the 2-D SDM.

Table III shows the results obtained with the refinement process and their comparisons for the case studies #1F and #2F. For both the cases, the RMSE obtained by the present method is identical to the best documented in the literature till now, which shows the uniqueness in the parameters obtained by the present method. For the case study #1F, the CC with refinement is 2/18 for this method, 16/138 by Laudani method, 8/36 by Cárdenas method, and 3/24 by Toledo method. Similarly for the case study #2F, the CC with refinement is 2/18 for this method, 28/204 by Laudani method, 27/141 by Cárdenas method, and 8/54 by Toledo method. In both cases, the CC with refinement

TABLE I
BASE VALUES, EXNLM PARAMETERS, AND INITIAL GUESSES FOR THE CASE STUDIES #1F, #2F, #3F, AND #4F

Case study	V_H (V)	I_H (A)	R (Ω)	a	b	c	d	n_0	r_{s0} (pu)	r_{sh0} (pu)
#1F	0.5900	0.7640	0.772251	-0.8208268	11.5733581	-0.0435190	1.0004404	1.8446965	0.1393631	159.039410
#2F	17.4885	1.0345	16.90526	-0.9314030	7.1851025	0.0295418	0.9997769	2.3298568	0.1749033	70.102124
#3F	21.02	1.663	12.63980	-0.9718192	11.9863218	-0.0281808	1	1.7437213	0.1372839	83.822479
#4F	19.21	7.48	2.568181	-1.0152827	9.2441561	0.0152827	1	2.0410987	0.1585989	117.59292

TABLE II
PARAMETERS (WITHOUT REFINEMENT) OBTAINED WITH THE 3-D PUSDM AND THEIR COMPARISON FOR THE CASE STUDIES #1F AND #2F

	Case study #1F			*Case study #2F*		
	Laudani (2B) [18]	**Cárdenas (2a) [19]**	**This work (stage-II)**	**Laudani (1B) [18]**	**Cárdenas (1a) [19]**	**This work (stage-II)**
I_{ph} **(pu)**	-	-	0.9957056	-	-	0.9990434
I_{ph} **(A)**	0.761060	0.760788	0.7607191	1.033537	1.032345	1.0335104
I_0 **(pu)**	-	-	4.3449899E-7	-	-	2.5381450E-6
I_0 **(μA)**	0.290125	0.3106845	0.3319572	2.825571	2.515158	2.6257110
R_s **(pu)**	-	-	0.0467865	-	-	0.0724446
R_s **(Ω)**	0.036800	0.036547	0.0361310	1.224053	1.238972	1.2246947
R_{sh} **(pu)**	-	-	70.2981791	-	-	40.4322493
R_{sh} **(Ω)**	49.973561	52.890463	54.2878608	689.321	747.94315	683.5180201
n	1.470097	1.477105	1.4837043	1.329426	1.317240	1.3216167
RMSE	8.8437E-4	7.7301E-4	8.0737695E-4	2.1547E-3	2.0468E-3	2.1726166E-3
CC	7/40	7/24	8/36	10/54	10/33	9/40

TABLE III
PARAMETERS (WITH REFINEMENT) OBTAINED WITH THE 5-D PUSDM AND THEIR COMPARISON FOR THE CASE STUDIES #1F AND #2F

	Case study #1F				*Case study #2F*			
	Laudani (2D) [18]	**Cárdenas (2b) [19]**	**Toledo (refined TSLLS) [21]**	**This work (stage-III)**	**(1D) [18]**	**Cárdenas (1b) [19]**	**Toledo (refined TSLLS) [21]**	**This work (stage-III)**
I_{ph} **(pu)**	-	-	-	0.9957958	-	-	-	0.9979533
I_{ph} **(A)**	0.7607884	0.760788	0.76078797	0.7607880	1.0323759	1.032377	1.0323823	1.0323827
I_0 **(pu)**	-	-	-	4.0666019E-7	-	-	-	2.4289115E-6
I_0 **(μA)**	0.3102482	0.3106847	0.31068485	0.3106884	2.5188848	2.517957	2.5129059	2.5127089
R_s **(pu)**	-	-	-	0.0473251	-	-	-	0.0733082
R_s **(Ω)**	0.3655304	0.036547	0.036546942	0.0365469	1.2390187	1.239060	1.2392888	1.2392956
R_{sh} **(pu)**	-	-	-	68.4881105	-	-	-	44.0493225
R_{sh} **(Ω)**	52.859056	52.890468	52.889804	52.8900296	745.6431	745.7122	744.71302	744.6655703
n	1.4769641	1.4771051	1.4771052	1.4771063	1.3174002	1.3173635	1.3171591	1.3171511
RMSE	7.7301E-4	7.7301E-4	7.730062726E-4	7.7300627E-4	2.0465E-3	2.0465E-3	2.0465347E-3	2.0465347E-3
CC	16/138	8/36	3/24	2/18	28/204	27/141	8/54	2/18
TCC	23/178	15/60	-	10/54	38/258	37/174	-	11/58

is the least by the present method. Further comparison is done in terms of the total CC (TCC) including CC without and with refinement. As shown in Table III, for the case study #1F, the TCC is 10/54 (the stages II + III) by this method, 23/178 [the solutions (2B) + (2D)] by Laudani method, 15/60 [the solutions (2a) + (2b)] by Cárdenas method. Similarly, for the case study #2F, the TCC is 11/58 (the stages II + III) by this method, 38/258 [the solutions (1B) + (1D)] by Laudani method, and 37/174 [the solutions (1a) + (1b)] by Cárdenas method. The least TCC by this method is a remarkable achievement, and this may be due to the adoption of the PUSDM instead of the SDM and the use of the 3-D form instead of the 2-D for the present method. Fig. 2 compares the experimental *I–V* curves with those obtained by the proposed method for the case studies #1F and #2F. The modeled curve exactly passes through all experimental data points for both the case studies. The visual coincidence of the curves further proves the ability of the proposed method for precise parameter extraction.

The results for the other two case studies #3F and #4F and their comparison with the Toledo method obtained from [32] are illustrated in Table IV. With the refinement, the five parameters are almost the same by both methods. Furthermore, the RMSE values without refinement are slightly on the higher side than those obtained with refinement. For the case study #3F, the RMSE correct up to seven digits (0.0017219) is obtained with the CC 1/12 by the present method against 8/54 by the Toledo method. Similarly, for the case study #4F, the RMSE correct up to four digits (0.0142) is obtained with the CC 1/12 by the present method against 11/72 by the Toledo method. Thus, the refined PV solution is achieved within the first step by the present method. In addition, the TCC for the case study #3F is 8/44 and for the case study #4F is 6/36. However, the Toledo method takes 8/54 for the case study #3F and 11/72 for the case study #4F. This clearly indicates that the present method has (two stages) TCC lower than (single stage) CC in comparison with the Toledo method.

TABLE IV
PARAMETERS (WITH AND WITHOUT REFINEMENT) OBTAINED WITH THE 3-D AND 5-D PUSDM, AND THEIR COMPARISON FOR THE CASE STUDIES #3F AND #4F

	Case study #3F			*Case study #4F*		
	This work (stage-II)	**This work (stage-III)**	**Toledo (refined TSLLS) [21]**	**This work (stage-II)**	**This work (stage-III)**	**Toledo (refined TSLLS) [21]**
I_{ph} **(pu)**	1.0002570	1.0005429	-	1.0004068	0.9993656	-
I_{ph} **(A)**	1.6634275	1.6639029	1.6639035	7.4830428	7.4752544	7.4752843
I_0 **(pu)**	1.0741764E-6	1.0472612E-6	-	2.5084794E-7	2.585525E-7	-
I_0 **(μA)**	1.7863553	1.7415953	1.741245	1.8763426	1.933973	1.9308835
R_s **(pu)**	0.0119725	0.0121552	-	0.0657738	0.0657632	-
R_s **(Ω)**	0.1513306	0.1536392	0.153640267	0.1689192	0.1688919	0.168918214
R_{sh} **(pu)**	46.6129863	45.360900	-	161.8583578	212.6960595	-
R_{sh} **(Ω)**	589.1791771	573.3530097	573.533748	415.6816915	546.2421092	570.189132
n	1.5231010	1.5203188	1.5202992	1.2419333	1.2444467	1.2443189
RMSE	0.0017310	0.0017220	0.0017219	0.0143522	0.0142931	0.0142516
CC	7/32	1/12	8/54	5/24	1/12	11/72

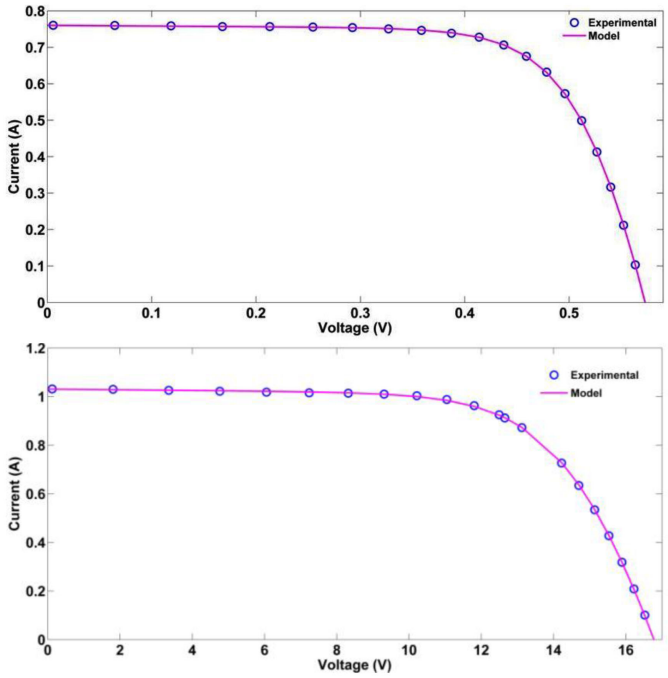

Fig. 2. Experimental and modeled *I–V* curves for the case studies #1F (top) and #2F (bottom).

B. PV Solution With Partial I–V Curves

In order to study the present method with the partial *I–V* curves, the data for the case studies #1P and #2P are selected from [19] and that for the case studies #3P and #4P are selected from [31]. The results obtained by the present method and the Toledo method [32] are represented in Table V. For example, the case study #1P exhibits the RMSE the same as the Toledo method to six decimal places (0.000469) with the CC 2/18 against 60/366 by the Toledo method, which is extremely low. Moreover, the single-stage refinement by the Toledo method takes 60/366, whereas the two-stage refinement by the present method takes 5/34, which indicates that the CC by the present method is extremely low. The similar trend is also observed in the other three case studies (13/72 (the present method) against 83/504 (the Toledo method) for the case study #2P, 20/116 against 32/198 for the case study #3P and 16/92 against 83/504 for the case study #4P). Therefore, the present method without and with refinement are the most suitable PV solution methods when a partial *I–V* curve is available. Here, one more noticeable difference is in the parameters obtained by the full and partial *I–V* curves for all four case studies. This can be further justified by performing an error analysis in the MPP obtained by the full and partial curves. Table VI illustrates the MPP parameters by the full and partial curves for four case studies. It is observed that though the five parameters are different, the MPP parameters deviate slightly obtained by the partial curve than those by the full curve. Amongst the error in MPP power ($E_{MP(P)}$), the highest error is 0.095819% for the case study #2 amongst the four case studies. Therefore, the performance of the present method is also acceptable in the case of partial curves availability during on-site measurements.

V. PV SOLUTION WITH SYNTHETIC *I–V* CURVES

In this section, the response of the present method to the synthetic *I–V* curves generated by the known five parameters is examined. Additional following four case studies are chosen for this purpose: (i) *Case study* #5: the known parameters at the STC of a multicrystalline Kyocera PV module KC200GT [33], (ii) *Case study* #6: the known parameters at the STC of a monocrystalline Shell PV module SQ160-PC [33], (iii) *Case study* #7: the known parameters at the STC of a thin-film Shell PV module ST40 [33], and (IV) *Case study* #8: the known parameters of BP SOLAR PV module BP-380 [34]. In all these case studies, the synthetic curves are reconstructed using the Lambert W function shown in (2b) with the help of the known parameters.

The *I–V* curves are generated with 341, 441, and 241 data points for the case studies #5, #6, and #7, respectively. The percent error in the estimated parameters with respect to the reference parameters and the RMSE are shown in Table VII for the case studies #5, #6, and #7 at the STC. The extremely low errors show that the estimated five parameters are exactly the same as the reference parameters, and the RMSE is extremely low with the highest value of the order 10^{-8} for the case study #5. Referring to the CC, the refined results are obtained at the end of the stage-II for the case study #5 and within the first iteration with CC 1/12 for the case studies #6 and #7. The analysis is

TABLE V
PARAMETERS (WITH AND WITHOUT REFINEMENT) OBTAINED WITH THE 3-D AND 5-D PUSDM, AND THEIR COMPARISON FOR THE CASE STUDIES #1P, #2P, #3P, AND #4P

	Case study #1P			*Case study #2P*		
	This work (stage-II)	**This work (stage-III)**	**Toledo (refined TSLLS) [21]**	**This work (stage-II)**	**This work (stage-III)**	**Toledo (refined TSLLS) [21]**
I_{ph} **(A)**	0.7648354	0.7653773	0.7655155	1.0189104	1.0191418	1.0248419
I_0 **(μA)**	3.2380785E-1	2.9926694E-1	2.8457869E-1	2.4282066	2.493842	1.2726724
R_s **(Ω)**	0.0307367	0.0315458	0.0321412	1.3008477	1.2975984	1.451360484
R_{sh} **(Ω)**	30.7324636	29.2424296	28.833148	11734.981	29954.00996	1531.884348
n	1.4745609	1.4673287	1.462824	1.3142429	1.3166575	1.2549738
RMSE	0.0004713	0.0004689	0.0004692	0.0014791	0.0012749	0.0012781
CC	3/16	2/18	60/366	8/36	5/56	83/504
	Case study #3P			*Case study #4P*		
I_{ph} **(A)**	1.6632072	1.6632328	1.6633908	7.4800990	7.4487700	7.4669833
I_0 **(μA)**	2.8821448	2.8943754	2.8050622	1.1444615	0.94769	0.51492263
R_s **(Ω)**	0.0042252	0.0030235	0.010067345	0.1868755	0.1984404	0.215781858
R_{sh} **(Ω)**	604.2180864	604.4797336	597.085488	428.6795545	5366.577955	489.865644
n	1.5695107	1.5699175	1.5665651	1.2055308	1.1938237	1.1523145
RMSE	0.0017730	0.0017728	0.0017721	0.0139045	0.0123486	0.0123157
CC	7/32	13/84	32/198	7/32	9/60	83/504

TABLE VI
MPP ERROR ANALYSIS BETWEEN THE FULL AND PARTIAL *I–V* CURVES OBTAINED BY THE PRESENT METHOD FOR THE CASE STUDIES #1 TO #4

Case study	$V_{MP(F)}$ **(V)**	$I_{MP(F)}$ **(A)**	$P_{MP(F)}$ **(W)**	$V_{MP(P)}$ **(V)**	$I_{MP(P)}$ **(A)**	$P_{MP(P)}$ **(W)**	$E_{MP(P)}$ **(%)**
#1	0.4506853	0.6893828	0.3106947	0.4513941	0.6884873	0.3107791	0.027178
#2	12.6552471	0.9126535	11.5498556	12.6365966	0.9148763	11.5609226	0.095819
#3	16.9749925	1.4996283	25.4561798	16.9883452	1.4984278	25.4558092	0.001456
#4	14.9215162	6.8205658	101.7731826	14.9059659	6.8330380	101.8530307	0.078457

TABLE VII
ERROR IN PARAMETERS (WITH REFINEMENT) OBTAINED WITH THE 5-D PUSDM FROM THE SYNTHETIC CURVES OF THE CASE STUDIES #5, #6, #7, AND #8

Case study	I_{ph} **(%)**	I_0 **(%)**	n **(%)**	R_s **(%)**	R_{sh} **(%)**	**RMSE**
***#5* (STC)**	3.2833E-6	0.00	1.9671E-7	1.2071E-7	8.3731E-5	2.0142201E-8
***#6* (STC)**	0.00	0.00	0.00	0.00	3.9484E-8	6.5067517E-12
#7 **(STC)**	7.4249E-12	0.00	2.6567E-11	1.2784E-11	5.9475E-9	2.1219741E-12
***Case study #8* with four different curves (average values)**						
#8	2.8406E-7	1.5456E-7	7.8701E-9	1.7189E-9	1.9328E-6	6.0901E-9
***Case study #8* with every 3 min curves within an hour (average values)**						
#8	5.4873E-8	0.00	2.1193E-9	8.0230E-10	7.5595E-6	1.9118E-9

further extended to extract the five parameters under different solar intensities and temperatures for these case studies. For this purpose, 35, 45, and 25 *I–V* data points are reconstructed at the STC using the reference parameters for the case studies #5, #6, and #7, respectively. Then, the data are transformed to different intensities and temperatures using the PV module datasheet information as shown in [35]. The intensity is changed from 200 to 1000 W/m^2 in a step-size 200 W/m^2 and the temperature from 25 to 75 °C with a step-size 25 °C. Once again, the RMSE is observed as lowest as of the order 10^{-12} in many cases. Also, a common observation is made that the refined parameters are obtained within the stage-II for the few cases and within the first iteration for the others. Thus, the present method capability is validated through a total number of 27 synthetic *I–V* curves.

An additional case study #8 with a set of five parameters at different conditions from [34] is used to obtain the synthetic curves (231 *I–V* data points in all curves). The parameters extraction is performed on the four curves at different hours with different intensities and the 16 curves taken every 3 min within an hour. Here, a common operating temperature 47 °C is considered for all curves from the datasheet [36] of the case study #8. As illustrated in Table VII, the extremely low average % error in all the parameters shows that the five parameters are precisely estimated and the resulted RMSE has the lowest value of the order 10^{-15}. As mentioned previously, here the refined parameters are obtained in stage-II for few cases and within the first iteration for the rest synthetic curves. Thus, the total 20 synthetic curves for this case study further prove the validity of the present method.

VI. CONCLUSION

On one hand, the PV parameters extraction related research works generally use the SDM quantities with their actual units, whereas work proposed here opts for the p.u. computation. Therefore, a stepwise SDM conversion into the 3-D and 5-D PUSDM is derived. In the initial stage, the equivalence between the 3-D PUSDM and the EXNLM is established which leads to allocate an appropriate initial guess for n. Two slopes defined by the extreme two consecutive points set the initial values for the

resistances for the 3-D PUSDM. Thus, it is concluded that the procedure with a single *I–V* curve input manages to self-compute the initial guesses, without any additional information about the PV module.

Furthermore, the 3-D and 5-D PUSDM conversions into the explicit functions are constructed with the help of the Lambert W function, which helps in the curve fitting. Considering four well-known case studies, the fitting between the 3-D PUSDM and the experimental *I–V* curve is performed. The results showed that the procedure up to this stage can also be considered for the parameter extraction as the RMSE and the CC are of a similar order in comparison with other equivalent published works. With the same case studies, the parameters are refined with the help of the 5-D PUSDM. All the parameters including the RMSE are in excellent agreement with the results obtained in the recent literatures. It is interesting to note that the refinement is obtained with the least CC ever published till now. When dealing with the partial *I–V* curves, the results obtained by the present method are with the lower RMSE and the lowest CC (for the stage-II and -III combined) in comparison with the last published work of the similar parameter extraction method. The estimated MPPs with the full and partial curves are also in excellent agreement. The claim of such promising results would go to the selection of the 3-D PUSDM instead of the 2-D (as used in two works of literature) and the pu computation.

Considering four well-known PV modules with the STC and non-STC conditions, the fitting between the PUSDM and the synthetic *I–V* curves is performed. The estimated parameters, the same as the known one, result in extremely low RMSE between two curves. Furthermore, the convergence is obtained within the stage-II or a single iteration in the stage-III.

Final recommendations to the PV research community are the PUSDM can be adopted in place of the SDM to reduce the computation complexity. For parameter extraction, one can opt the procedure up to the second stage in case the accuracy requirement is not strict otherwise go with the refinement stage. It is hoped that the method will be useful for the development of new model-based MPPT algorithms for onsite PV operations in which limited information about *I–V* curve is available. A single-page MATLAB script is made available to the interested researchers through e-mail communication to the author.

ACKNOWLEDGMENT

The author was inspired to develop this work through an e-mail communication from Prof. Muhammad Ashraful Alam of the Purdue University, USA. The author is grateful to his students Vishal Chouhan and Rishil Shah for setting the MATLAB code sequence.

REFERENCES

[1] R. Asadpour, X. Sun, and M. A. Alam, "Electrical signatures of corrosion and solder bond failure in c-Si solar cells and modules," *IEEE J. Photovolt.*, vol. 9, no. 3, pp. 759–767, May 2019.

[2] H. K. Mehta, H. Warke, K. Kukadiya, and A. K. Panchal, "Accurate expressions for single-diode-model solar cell parameterization," *IEEE J. Photovolt.*, vol. 9, no. 3, pp. 803–810, May 2019.

[3] P. Bharadwaj and V. John, "Subcell modeling of partially shaded photovoltaic modules," *IEEE Trans. Ind. Appl.*, vol. 55, no. 3, pp. 3046–3054, May/Jun. 2019.

[4] M. H. Deihimi, R. A. Naghizadeh, and A. Fattahi Meyabadi, "Systematic derivation of parameters of one exponential model for photovoltaic modules using numerical information of data sheet," *Renewable Energy*, vol. 87, pp. 676–685, 2016.

[5] X. Ma *et al.*, "Data-Driven *I–V* feature extraction for photovoltaic modules," *IEEE J. Photovolt.*, vol. 9, no. 5, pp. 1405–1412, Sept. 2019.

[6] H. M. Waly, H. Z. Azazi, D. S. M. Osheba, and A. E. El-Sabbe, "Parameters extraction of photovoltaic sources based on experimental data," *IET Renewable Power Gener.*, vol. 13, no. 9 pp. 1466–1473, 2019.

[7] A. H Sabry, W. Z. W. Hasan, Y. H. Sabri, and M. Z. A. Ab-Kadir, "Silicon PV module fitting equations based on experimental measurements," *Energy Sci. Eng.*, vol. 7, no. 1, pp. 132–145, 2019.

[8] X. Chen and Y. Kunjie, "Hybridizing cuckoo search algorithm with biogeography-based optimization for estimating photovoltaic model parameters," *Sol. Energy*, vol. 180, pp. 192–206, 2019.

[9] S. J. Patel, A. K. Panchal, and V. Kheraj, "Extraction of solar cell parameters from a single current–voltage characteristic using teaching learning based optimization algorithm," *Appl. Energy*, vol. 119, pp. 384–393, 2014.

[10] I. A. Ibrahim, J. Hossain, B. C. Duck, and C. J. Fell, "An adaptive wind driven optimization algorithm for extracting the parameters of a single-diode PV cell model," *IEEE Trans. Sustain. Energy*, vol. 11, no. 2, pp. 1054–1066, Apr. 2020.

[11] Z. Yan, C. Li, Z. Song, L. Xiong, and C. Luo, "An improved brain storming optimization algorithm for estimating parameters of photovoltaic models," *IEEE Access*, vol. 7, pp. 77629–77641, 2019.

[12] U. Jadli, P. Thakur, and R. D. Shukla, "A new parameter estimation method of solar photovoltaic," *IEEE J. Photovolt.*, vol. 8, no. 1, pp. 239–247, Jan. 2018.

[13] N. Muangkote, K. Sunat, S. Chiewchanwattana, and S. Kaiwinit, "An advanced onlooker-ranking-based adaptive differential evolution to extract the parameters of solar cell models," *Renewable Energy*, vol. 134, pp. 1129–1147, 2019.

[14] H. Sheng *et al.*, "Parameters extraction of photovoltaic models using an improved moth-flame optimization," *Energies*, vol. 12, no. 18, 2019, Art. no. 3527.

[15] J. D. Bastidas-Rodriguez, G. Petrone, C. A. Ramos-Paja, and G. Spagnuolo, "A genetic algorithm for identifying the single diode model parameters of a photovoltaic panel," *Math. Comput. Simul.*, vol. 131 pp. 38–54, 2017.

[16] A. Laudani, F. R. Fulginei, and A. Salvini, "Identification of the one-diode model for photovoltaic modules from datasheet values," *Sol. Energy*, vol. 108, pp. 432–446, 2014.

[17] C. Zhang, J. Zhang, Y. Hao, Z. Lin, and C. Zhu, "A simple and efficient solar cell parameter extraction method from a single current-voltage curve," *J. Appl. Phys.*, vol. 110, no. 6, 2011, Art. no. 064504.

[18] A. Laudani, F. R. Fulginei, and A. Salvini,. "High performing extraction procedure for the one-diode model of a photovoltaic panel from experimental *I–V* curves by using reduced forms," *Sol. Energy*, vol. 103, pp. 316–326, 2014.

[19] A. A. Cárdenas, M. Carrasco, F. Mancilla-David, A. Street, and R. Cárdenas, "Experimental parameter extraction in the single-diode photovoltaic model via a reduced-space search," *IEEE Trans. Ind. Electron.*, vol. 64, no. 2, pp. 1468–1476, Feb. 2017.

[20] L. H. I. Lim, Z. Ye, J. Ye, D. Yang, and H. Du, "A linear identification of diode models from single *I–V* characteristics of PV panels," *IEEE Trans. Ind. Electron.*, vol. 62, no. 7, pp. 4181–4193, Jul. 2015.

[21] F. J. Toledo, J. M. Blanes, and V. Galiano, "Two-step linear least-squares method for photovoltaic single-diode model parameters extraction," *IEEE Trans. Ind. Electron.*, vol. 65, no. 8, pp. 6301–6308, Aug. 2018.

[22] H. Saadat, *Power System Analysis*, New Delhi, India: Tata McGraw-Hill, 2004, ch. 3, pp. 88.

[23] K. Lappalainen, P. Manganiello, M. Piliougine, G. Spagnuolo, and S. Valkealahti, "Virtual sensing of photovoltaic module operating parameters," *IEEE J. Photovolt.*, vol. 10, no. 3, pp. 852–862, May 2020.

[24] G. Spagnuolo, K. Lappalainen, S. Valealahti, and P. Manganiello, "Identification and diagnosis of a photovoltaic module based on outdoor measurements," in *Proc. IEEE Milan PowerTech*, 2019, pp. 1–6.

[25] L. Liu, W. Liu, X. Zhang, and J. Ingenhoff, "Research on the novel explicit model for photovoltaic IV characteristic of the single diode model under different splitting spectrum," *Results Phys.*, vol. 12, pp. 662–672, 2019.

[26] B. S. Grewal, *Numerical Methods in Engineering and Science: C, C++ and MATLAB*. Dulles, VA, USA: Mercury Learning and Information, Ch. 1, pp. 4, 2019.
[27] D. Sera, R. Teodorescu, and P. Rodriguez, "PV panel model based on datasheet values," in *Proc. IEEE Int. Symp. Ind. Electron.*, 2007, pp. 2392–2396.
[28] X. Gao, Y. Cui, J. Hu, N. Tahir, and G. Xu, "Performance comparison of exponential, Lambert W function and special trans function based single diode solar cell models," *Energy Convers. Manage.*, vol. 171, pp. 1822–1842, 2018.
[29] R. M. Corless, G. H. Gonnet, D. E. G. Hare, D. J. Jeffrey, and D. E. Knuth, "On the Lambert W function," *Adv. Comput. Math.*, vol. 5, no. 1, pp. 329–359, 1996.
[30] T. Easwarakhanthan, J. Bottin, I. Bouhouch, and C. Boutrit, "Nonlinear minimization algorithm for determining the solar cell parameters with microcomputers," *Int. J. Sol. Energy*, vol. 4, pp. 1–12, 1986.
[31] N. T. Tong and W. Pora, "A parameter extraction technique exploiting intrinsic properties of solar cells," *Appl. Energy*, vol. 176, pp. 104–15, 2016. [Online]. Available: http://dx.doi.org/10.1016/j.apenergy.2016.05.064
[32] [Online]. Available: pvmodel.umh.es. Assessed on: Dec 1, 2019.
[33] H. Mokhliss, A. El-Amiri, and K. Rais, "Estimation of five parameters of photovoltaic modules using a synergetic control theory approach," *J. Comput. Electron.*, vol. 18, no. 1, pp. 241–250, 2019.
[34] R. Gutiérrez, J. M. Blanes, D. Marroquí, A. Garrigós, and F. J. Toledo, "System-on-chip for real-time satellite photovoltaic curves telemetry," *IEEE Trans. Ind. Inform.*, vol. 14, no. 3, pp. 951–957, Mar. 2017.
[35] T. T. Yetayew and T. R. Jyothsna, "Improved single-diode modeling approach for photovoltaic modules using data sheet," in *Proc. Annu. IEEE India Conf.*, 2013, pp. 1–6.
[36] Datasheet for 80 W photovoltaic module BP 380 from BP solar, 2008.